

Performance evaluation of soil-embedded plastic optical fiber sensors for geotechnical monitoring

Cheng-Cheng Zhang^{1a}, Hong-Hu Zhu^{*1,2}, Bin Shi^{1b}, Jun-Kuan She^{1c} and Dan Zhang^{1d}

¹*School of Earth Sciences and Engineering, Nanjing University, Nanjing 210023, China*

²*Nanjing University High-tech Institute at Suzhou, Suzhou 215123, China*

(Received June 7, 2015, Revised December 8, 2015, Accepted December 17, 2015)

Abstract. Based on the distributed fiber optic sensing (DFOS) technique, plastic optical fibers (POFs) are attractive candidates to measure deformations of geotechnical structures because they can withstand large strains before rupture. Understanding the mechanical interaction between an embedded POF and the surrounding soil or rock is a necessary step towards establishing an effective POF-based sensing system for geotechnical monitoring. This paper describes a first attempt to evaluate the feasibility of POF-based soil deformation monitoring considering the POF–soil interfacial properties. A series of pullout tests were performed under various confining pressures (CPs) on a jacketed polymethyl methacrylate (PMMA) POF embedded in soil specimens. The test results were interpreted using a fiber–soil interaction model, and were compared with previous test data of silica optical fibers (SOFs). The results showed that the range of CP in this study did not induce plastic deformation of the POF; therefore, the POF–soil and the SOF–soil interfaces had similar behavior. CP was found to play an important role in controlling the fiber–soil interfacial bond and the fiber measurement range. Moreover, an expression was formulated to determine whether a POF would undergo plastic deformation when measuring soil deformation. The plasticity of POF may influence the reliability of measurements, especially for monitored geo-structures whose deformation would alternately increase and decrease. Taken together, these results indicate that in terms of the interfacial parameters studied here the POF is feasible for monitoring soil deformation as long as the plastic deformation issue is carefully addressed.

Keywords: distributed geotechnical monitoring; soil deformation; plastic optical fiber (POF); plasticity; interfacial behavior

1. Introduction

Nowadays researchers and practitioners rely more heavily on advanced detecting methods to understand the complex behavior of geo-materials, and to evaluate the performance of

*Corresponding author, Associate Professor, E-mail: zhh@nju.edu.cn

^a Graduate Student, E-mail: zhangchengcheng@gmail.com

^b Professor, E-mail: shibin@nju.edu.cn

^c Graduate Student, E-mail: mf1329019@smail.nju.edu.cn

^d Associate Professor, E-mail: zhangdan@nju.edu.cn

infrastructures built on them. The distributed fiber optic sensing (DFOS) technique enables distributed strain measurement along an optical fiber over dozens of kilometers while maintaining relatively high degrees of accuracy and spatial resolution, which shows great potential in the field of geotechnical monitoring (Mohamad *et al.* 2012, Zhu *et al.* 2012, Feng *et al.* 2015). Over the past two decades, considerable progress has been made in applying DFOS systems to monitor the deformation of a variety of geotechnical structures (Habel and Krebber 2011). The distributed sensing fibers have been directly embedded in soil masses and successfully captured the process and pattern of ground settlements (Glisic and Yao 2012, Klar *et al.* 2014) and slope movements (Naruse *et al.* 2000, Iten *et al.* 2008, Olivares *et al.* 2009, Wang *et al.* 2009, Zhu *et al.* 2014, Sun *et al.* 2014, Zeni *et al.* 2015, Zhu *et al.* 2015). However, the frequently adopted silica-based sensing fibers may be limited in geo-engineering applications due to the low break-down strain of only 1% or a bit more (Habel and Krebber 2011, Leung *et al.* 2013). As noted by Zhang *et al.* (2015), large deformation measurements in the field or in laboratory model tests is of great importance for investigating the failure mechanism of soil structures. While efforts have been made to extend the measurement range of existing sensing fibers (e.g. Arifin *et al.* 2015), this problem remains one of the main barriers that constrain the application of DFOS technique to soil deformation monitoring.

Plastic or polymer optical fibers (POFs) are potentially superior alternatives to silica optical fibers (SOFs) for diverse geo-engineering applications, because of their low Young's moduli and high break-down strain limits. It has been reported that polymethyl methacrylate (PMMA) has an elastic limit around 10% (Large *et al.* 2015), and a standard PMMA-based POF can be stretched far more than their silica counterparts (up to 40%) without significant distortion of light guiding properties (Liehr *et al.* 2008, 2009). In the past decade, various POF sensors have been developed for structural and environmental monitoring (Abdi *et al.* 2008, Kuang *et al.* 2009, Peters 2011, Bilro *et al.* 2012, Morisawa and Muto 2012, Grassini *et al.* 2014, Kuang *et al.* 2015). It is noteworthy that POFs have attracted much interest for their tremendous potential in geotechnical monitoring (e.g. Habel and Krebber 2011). Among the recently published works, some researchers (Lenke *et al.* 2007, Krebber *et al.* 2008, Liehr *et al.* 2008, 2009) have developed several geotextile-embedded POF sensors for distributed geotechnical monitoring purposes. They have reported a maximum detectable strain of 6% for a textile-integrated PMMA POF sensor that was installed within a model box filled with layered sands. The survivability of the sensors has been further proved by installing the sensor-equipped geotextiles into a dam, a test dike, and a railway embankment. Despite the exciting results reviewed here, the use of POFs in deformation monitoring of soils and rocks is still limited.

Fig. 1 shows schematically how the lateral deformation of a soil layer is captured by a directly embedded POF sensor under a simple circumstance. The external pressure causes lateral movement of the soil layer, thereby inducing elongation of the fiber. Obviously, the reliability of measured data is concerned with the strain transfer from the soil to the sensing fiber, which is strongly dependent on the contact condition between the fiber and the soil. If the contact is not intimate, the collected data can barely reflect the actual strain of the soil. Therefore, understanding the interaction mechanism between a strain sensing fiber and the surrounding geo-material is a fundamental prerequisite for implementing reliable and effective DFOS-based geotechnical monitoring. In this aspect, a simplified interaction model has been proposed to characterize the interfacial behavior between fibers and natural geo-materials—soils (Zhang *et al.* 2014, 2015). The model was applied to interpret the results of several jacketed SOFs pulled out from sandy soils, where the influence of normal pressure was emphasized. For POFs, particular attention should be drawn to the interfacial effect because: 1) the Young's modulus of PMMA (3.2 GPa) is much lower

than silica (72 GPa), and 2) the POF undergoes a large amount of plastic deformation before breakage. However, research in this field has not been reported previously. To facilitate the application of POF sensors to geotechnical monitoring, a comprehensive study regarding the POF–soil interaction is urgently needed.

Our goal here is to understand the interfacial behavior between POF and soil, and to assess whether POFs are suitable for large deformation monitoring of soils. For this purpose, laboratory pullout tests were carried out under various confining pressures (CPs) on a 2.2 mm PMMA POF embedded in soil. The interfacial parameters of the POF were compared with previously reported data of SOFs. Additionally, the influence of plastic deformation of POF on geotechnical monitoring results was preliminarily discussed.

2. Methodology

2.1 Material

A commercially available POF (Mitsubishi’s GH4001 fiber) was tested in this study. The diameter of the PMMA core was 0.980 mm, and the thicknesses of the fluorinated cladding and polyethylene (PE) jacket were 0.02 mm and 1.2 mm, respectively. The PE jacket can protect the fiber from external physical and chemical influences, and add more mechanical strength to the fiber. This fiber has been used for several geotechnical monitoring applications (Liehr *et al.* 2008, 2009). Standard uniaxial tensile test was carried out to determine the tensile properties of the fiber. Fig. 2 plots the stress–strain curve of the fiber. The PE-jacketed PMMA fiber had an average Young’s modulus E of 0.522 GPa, and a yield strain (elastic limit) of 3.34%. Detailed parameters of the fiber are summarized in Table 1.

A sandy soil collected from a construction site in Xianlin District, Nanjing, China was used here. The soil was classified as SP (i.e., poorly graded sand) following the Unified Soil Classification System (USCS) (ASTM 1992). Grain size distribution of the soil is shown in Fig. 3. The average grain size of the sand was 0.510 mm, which is about a quarter of the outer diameter of the POF. Detailed properties of the sand were well characterized by Zhang *et al.* (2014).

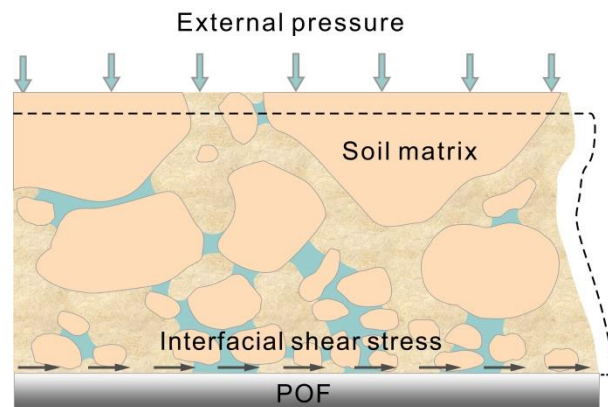


Fig. 1 Elongation of an embedded plastic optical fiber (POF) due to lateral deformation of a soil layer under external pressure

Table 1 Detailed properties of the test fiber

Outer diameter (mm)			Young's modulus (GPa)	Yield strain (%)	Yield strength (MPa)
Core	Cladding	Jacket			
0.980	1.00	2.20	0.522	3.34	18.4

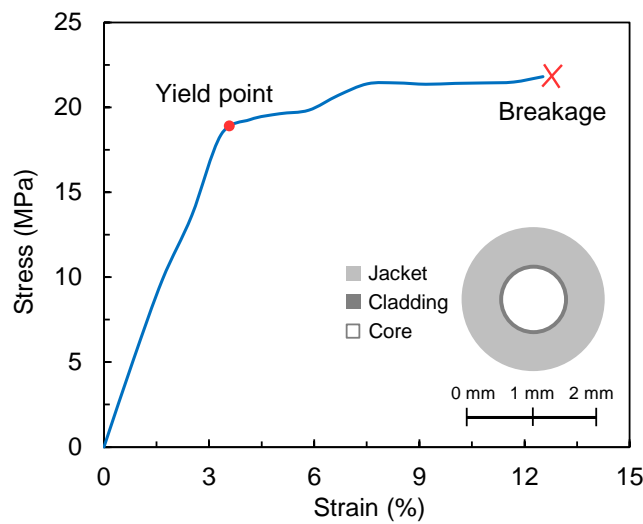


Fig. 2 Measured stress–strain curve for the polymethyl methacrylate (PMMA) POF. Sample length was 500 mm. Loading rate was 8.00 mm/min. Structure of the POF is shown at bottom right

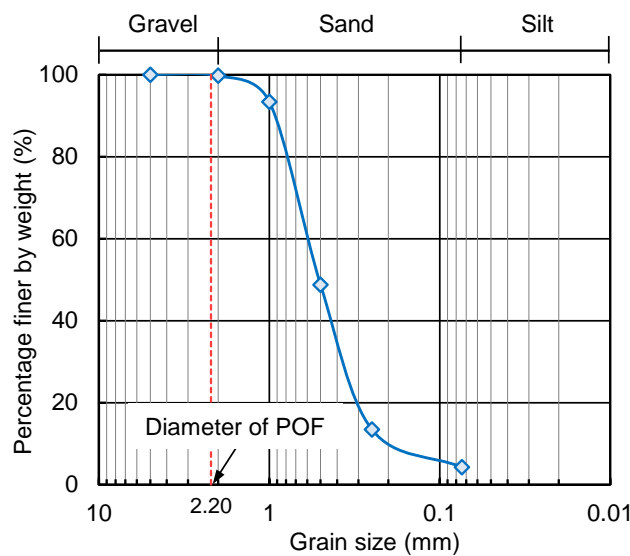


Fig. 3 Grain size distribution of the soil

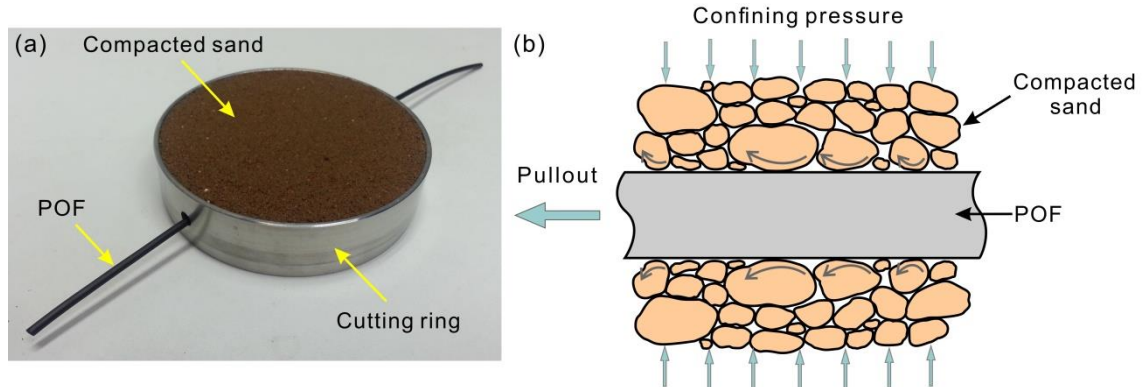


Fig. 4 (a) Photo of a prepared specimen to be tested; (b) schematic drawing of a POF being pulled out from compacted sand

2.2 Experimental program

The test specimens were prepared using the method reported by Zhang *et al.* (2014). The specimen contained a POF embedded within a cutting ring filled with compacted soil, with both ends passing through the holes drilled in the side walls. The diameter of the cutting ring was changed to 79.8 mm to obtain a longer fiber–soil bonding length. For all the specimens, the soil dry density was kept at 1.80 g/cm^3 , and the water content remained 10.0%. Fig. 4(a) shows a prepared specimen to be tested. Prior to testing, the specimens were allowed to equilibrate for 24 hours. Moreover, CPs ranging from 7.5 kPa to 90 kPa were used in the tests. The CPs were applied on the specimens by using a modified oedometer.

Afterward, the embedded POFs were pulled out from the specimens at a constant rate of 0.72 mm/min using a step motor. The pullout force and the pullout displacement were measured by a force gauge and a dial gauge, respectively. Fig. 4(b) schematically shows a POF being pulled out from compacted sand. The detailed test procedure can also be found in Zhang *et al.* (2014).

2.3 Determination of interfacial parameters

Using the procedure described in the previous section, the relationship between the pullout force and pullout displacement under each CP was obtained for this fiber. To analyze the interfacial properties, a recently proposed fiber–soil interaction model (Zhang *et al.* 2014) was applied separately to every pullout force–pullout displacement curve. Based on a tri-linear shear stress–displacement relationship of the fiber–soil interface (Fig. 5(a)), the model considered the progressive failure along the fiber–soil interface, and divided the whole pullout process into five consecutive phases. This methodology not only enables the determination of typical interfacial parameters, such as the interfacial shear strengths (τ_{\max} and τ_{res}) and interfacial shear stiffnesses (G_1 and G_2), but it also allows for analyzing the evolution of tensile force and interfacial shear stress. Through fitting the experimental curves, six parameters were determined, i.e. τ_{\max} , τ_{res} , G_1 , G_2 , u_{eff} , and u_{peff} . The meanings of τ_{\max} , τ_{res} , G_1 and G_2 are schematically shown in Fig. 5(a), whereas the effective displacement (u_{eff}) and the partially effective displacement (u_{peff}) are defined

as

$$\begin{cases} u_{\text{eff}} = \frac{\tau_{\text{max}}}{G_1} \\ u_{\text{peff}} = \frac{\tau_{\text{max}}}{G_1} + \frac{\tau_{\text{max}} - \tau_{\text{res}}}{G_2} + \frac{2\tau_{\text{res}}}{DE} L^2 \end{cases} \quad (1)$$

where D , L and E are the diameter, length and Young's modulus of the fiber, respectively. The two characteristic displacements can be used to assess the range of optical fiber sensor-based soil deformation measurement. Detailed explanation and discussion of the methodology can be found in Zhang *et al.* (2014, 2015).

3. Results and discussion

In this section, the mechanical properties of the POF–soil interface were compared with previous results of three SOF–soil interfaces reported in Zhang *et al.* (2015). The three fibers, SOF-1, SOF-2 and SOF-3, were standard jacketed SOFs. Their outer diameters were 0.900 mm, 1.20 mm, and 1.80 mm, respectively. Young's moduli were 1.75 GPa, 1.01 GPa, and 0.500 GPa, respectively. Of note, the POF–soil interface and the SOF–soil interfaces were tested under the same experimental conditions (except for slight difference in the CP range).

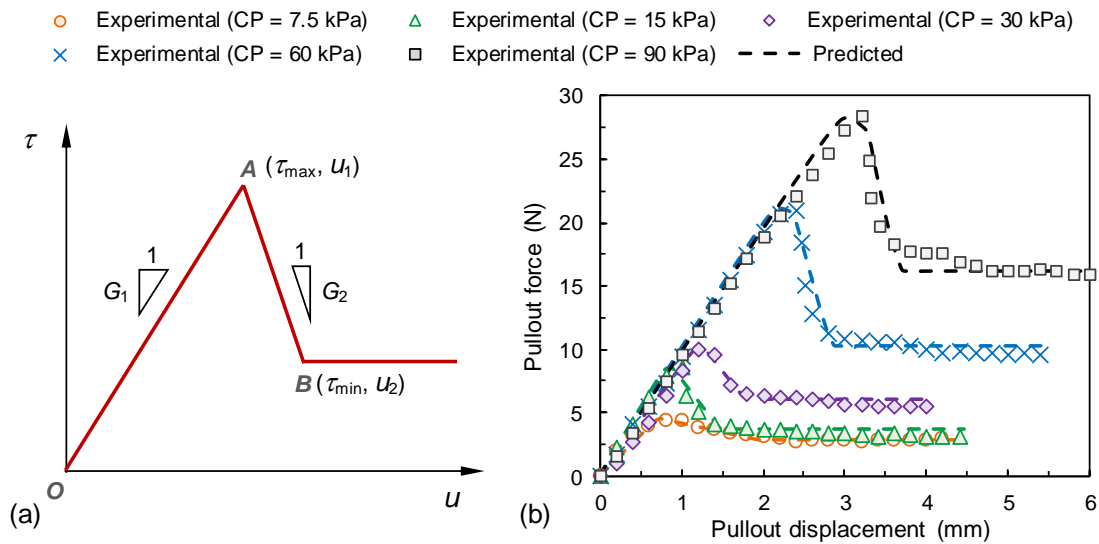


Fig. 5 (a) A tri-linear interfacial shear stress-displacement relationship for deriving the simplified fiber–soil interaction model (Zhang *et al.* 2014); (b) Experimental and predicted pullout force–pullout displacement curves. Confining pressure (CP) varied from 7.5 kPa to 90 kPa. Dashed lines denote results predicted by the model

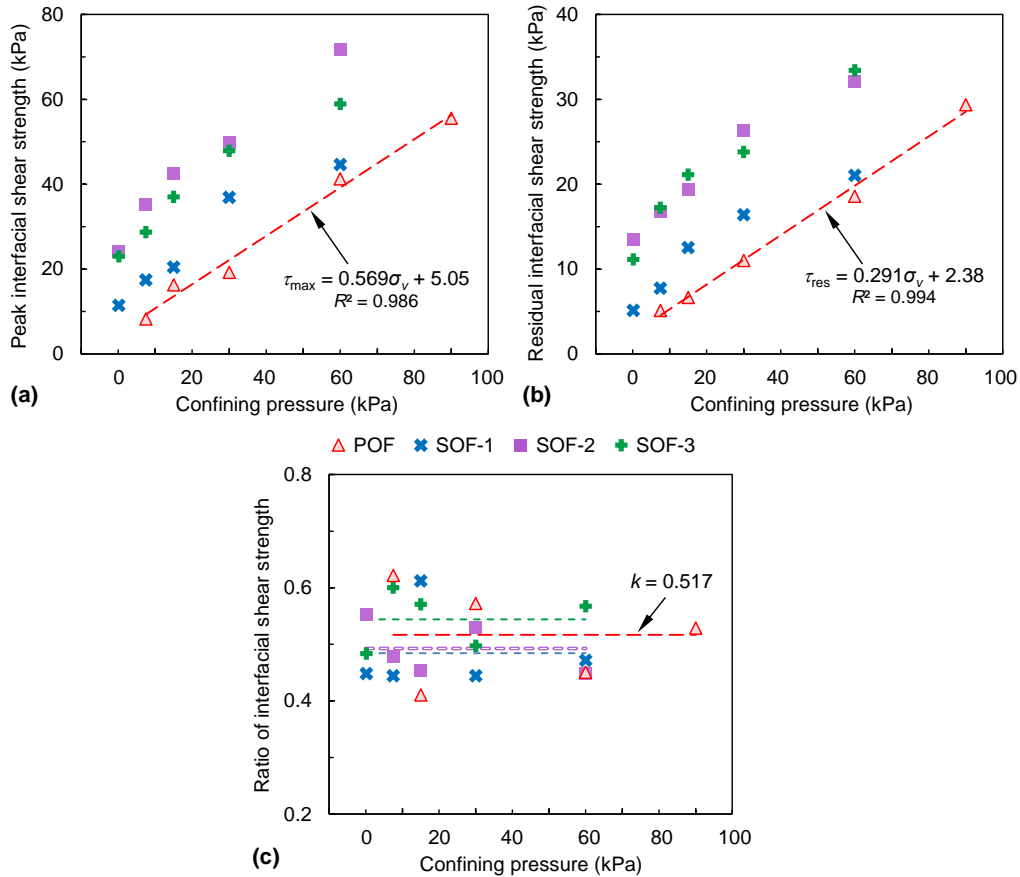


Fig. 6 Comparison of interfacial parameters between POF and silica optical fiber (SOF) under different CPs: (a) peak interfacial shear strength; (b) residual interfacial shear strength; (c) ratio of interfacial shear strength. Dashed lines indicate linear fits in (a) and (b), and constant fits in (c)

3.1 Characteristics of pullout force–pullout displacement curves

Pullout force–pullout displacement curves obtained from the tests, together with predictions from the interaction model, are plotted in Fig. 5(b). It is shown that the predictions agreed well with the experimental data, indicating that the interaction model is applicable to various fibers. However, we note that the final downtrend of the experimental curves was not captured by the model because a constant residual interfacial shear strength was assumed for the sake of simplicity (Zhang *et al.* 2014). To perform more accurate modeling, it is suggested that one more parameter should be introduced to account for this effect. Additionally, these curves showed similar shapes under different CPs: firstly, the pullout force increased approximately linearly with the pullout displacement up to the peak value; afterwards, the pullout force decreased notably, especially for that under the high CP; finally, the pullout force remained stable with a slight downtrend. These characteristics are consistent with the three SOF–soil interfaces (Zhang *et al.* 2015).

3.2 Analysis of interfacial parameters

Parameters of the POF–soil interface under different CPs obtained by the simplified fiber–soil interaction model are shown in Figs. 6–8. Similar to the three SOF–soil interfaces, both the peak and residual interfacial shear strengths, τ_{\max} and τ_{res} , of the POF–soil interface increased almost linearly with increasing confining pressure (Figs. 6(a) and 6(b)). This indicates high CPs can enhance the interfacial bond between the POF and the surrounding soil; however, the interfacial bond was slightly looser when compared to the SOFs. Because the influence of CP on the ratio of interfacial shear strength, defined as $k = \tau_{\text{res}} / \tau_{\max}$, was not evident (Fig. 6(c)), a constant fit would be preferable in this case. The POF–soil interface had an average value of 0.517, which fell in the range of the SOF data (0.484–0.544). Zhang *et al.* (2015) suggested a low value of k for engineering practices so that it would be easier to identify the working state of a strain sensing fiber. At this point, however, the POF showed no difference in this parameter as compared to the SOF.

Fig. 7 displays the comparisons of interfacial shear stiffnesses, G_1 and G_2 , between the POF and the SOF. The influence of CP on G_1 appeared to be difficult to assess (Fig. 7(a)). Previous SOF data showed that increased CP could either slightly increase, slightly decrease, or leave unchanged the values of G_1 . These results, taken together, suggest that the impact of CP on the interfacial shear stiffness G_1 may be minor. The constant fit showed that G_1 of the POF–soil interface had an average value of 18.5 MPa/m, which was smaller than those for the SOFs. This indicates that the POF–soil interface is easier to deform than the SOF–soil interface when subjected to shear. Notably, the impact of CP on G_2 was more pronounced compared to G_1 (Fig. 7(b)), suggesting that pullout may contribute to disturbance to the interfacial soil structure. While soil particles were reported to rotate and rearrange at the fiber surface under shear (Tang *et al.* 2010, Zhang *et al.* 2015), to what extent the microscopic effect caused the difference between G_1 and G_2 remains to be elucidated.

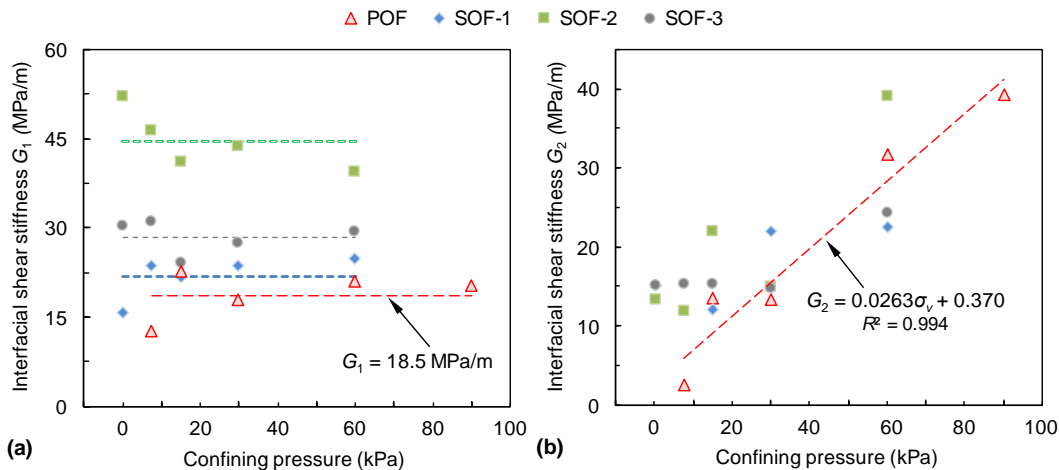


Fig. 7 Comparison of interfacial parameters between POF and SOF under different CPs: (a) interfacial shear stiffness G_1 ; (b) interfacial shear stiffness G_2 . Dashed lines indicate constant fits in (a), and linear fit in (b)

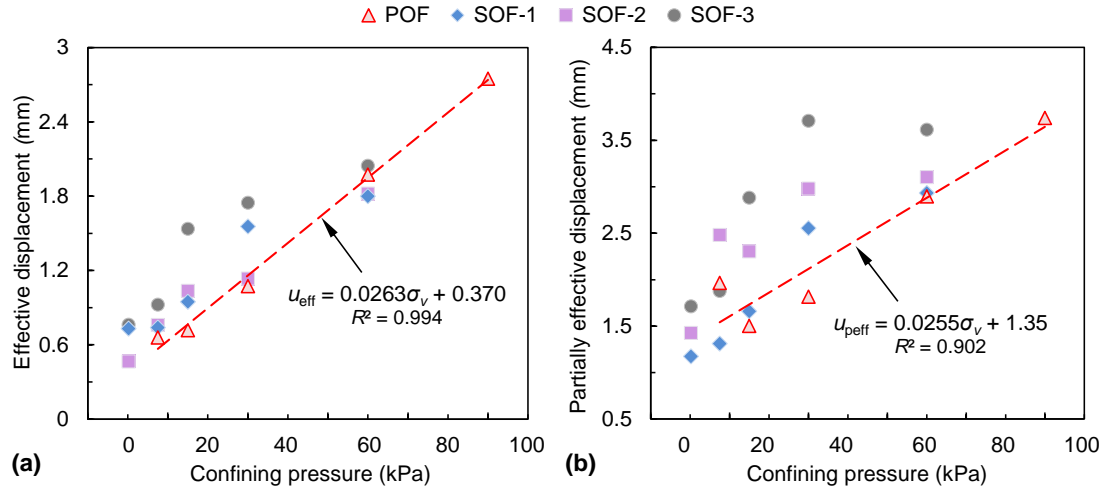


Fig. 8 Comparison of interfacial parameters between POF and SOF under different CPs: (a) effective displacement; (b) partially effective displacement. Dashed lines indicate linear fits

The comparisons of effective and partially effective displacements between the two interfaces are shown in Fig. 8. Similar to the three SOF–soil interfaces, both characteristic displacements increased almost linearly with the confining pressure, indicating high CPs can widen the measurement range of the POF. However, the two characteristic displacements of the POF were smaller as compared to the SOFs, although the difference appeared to be less significant at CP = 60 kPa. More data are needed to confirm this observation.

Overall, more similarities than differences were found between the POF–soil interface and the SOF–soil interface. One may question, however, why the marked difference in Young’s modulus between PMMA and silica did not contribute to different interfacial behaviors. One possible explanation is that the difference in average Young’s modulus was significantly decreased due to the external jackets. For instance, the POF and SOF-3 had almost the same value of Young’s modulus. Although the interfacial bond between SOF-3 and soil was tighter and the measurement range of SOF-3 was wider, both interfaces exhibited similar mechanical properties under the influence of CPs. At this stage it may be concluded that the mechanical behavior of a PMMA POF–soil interface is similar to a SOF–soil interface under the current experimental conditions. Further, these results reveal a fundamental role for CP in control of the fiber–soil interfacial bond and the fiber measurement range.

4. Critical issues in soil deformation monitoring

POFs as sensing fibers are attractive candidates for geotechnical monitoring, in large part because of the ability to measure large strains and deformations. Although POFs are capable of measuring strain up to 40% without marked distortion of light guiding properties (Habel and Krebber 2011), one might still question the reliability of measured data provided that the tensile stress in the fiber reaches the yield strength, thereby inducing plastic deformation. To explore this

issue, two questions should be addressed. One is under what conditions plastic deformation occurs, the other is how plastic deformation influences the measurements. Here some preliminary analysis is presented.

4.1 An expression for maximum tensile stress

In our experiments, the maximum tensile stress σ_{\max} of the POF was 7.44 MPa (Fig. 9; CP = 90 kPa), far smaller than the measured yield strength σ_y (Table 1; 18.4 MPa). Therefore, plastic deformation did not occur. Nevertheless, it is reasoned that a CP of 234 kPa would induce plastic deformation, according to the empirical relationship shown in Fig. 9. Apparently, this value is far beyond the CP range in this initial study. However, this value is common in geotechnical centrifuge model tests, such as modeling of soil slopes (Ling *et al.* 2009, Li *et al.* 2011) and embankments (Sharma *et al.* 2001). If POFs had been employed in these tests, the fibers might have experienced plastic deformations. Of note, CP is not the only factor that affects σ_{\max} . Other environmental factors such as moisture content and dry density of soil are also important (Tang *et al.* 2010). It is therefore necessary to derive an expression for σ_{\max} as functions of various parameters.

Based on the simplified fiber–soil interaction model (Zhang *et al.* 2014, 2015), the maximum pullout force F_{\max} is reached during Phase II, where both elastic and softening zones exist along the fiber. The pullout force F_0 in Phase II is derived as a function of the length of the softening zone L_s

$$F_0 = \pi D \tau_{\max} \left[\frac{\sin \alpha_2 L_s}{\alpha_2} + \frac{\tanh \alpha_1 (L - L_s) \cos \alpha_2 L_s}{\alpha_1} \right], \quad 0 \leq L_s \leq L \quad (2)$$

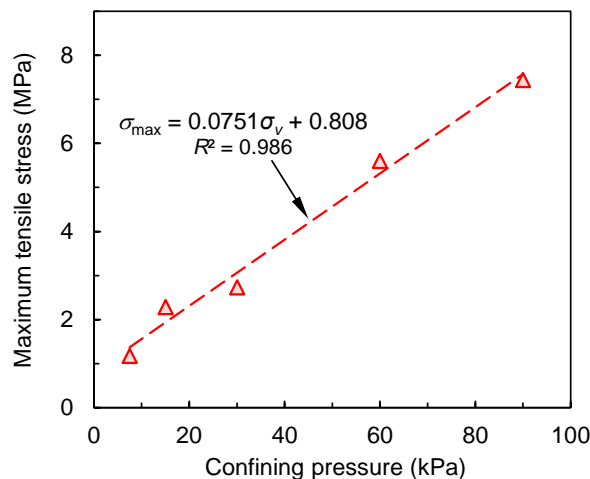


Fig. 9 Relationship between confining pressure and maximum tensile stress of the POF experienced during the pullout process. The dashed line indicates linear regression

where D and L are the diameter and length of the optical fiber, respectively; τ_{\max} is the peak interfacial shear strength; and $\alpha_i = \sqrt{4G_i / ED}$ ($i=1, 2$), with G_1 and G_2 being the interfacial shear stiffnesses, E being the Young's modulus of the optical fiber. Apparently, F_0 peaks when $dF_0 / dL_s = 0$. Combining it with Eq. (2) yields

$$\alpha_1 \tanh \alpha_1 (L - L_s) = \alpha_2 \tan \alpha_2 L_s, \quad 0 \leq L_s \leq L \quad (3)$$

To the best of our knowledge no exact analytical solution exists for Eq. (3). Therefore, this equation is approximated by using a Taylor-series expansion method. An approximate solution $L_s = G_1 L / (G_1 + G_2)$ is obtained with the relative error not exceeding 7.5% in any of our estimates. Substituting the approximate solution and Eq. (3) in Eq. (2) yields

$$F_{\max} = \frac{\pi D \tau_{\max} (\alpha_1^2 + \alpha_2^2)}{\alpha_2 \alpha_1^2} \sin \frac{L G_1 \alpha_2}{G_1 + G_2} \quad (4)$$

Substituting $\sigma_{\max} = F_{\max} / A$ in Eq. (4) yields

$$\sigma_{\max} = \frac{4 \tau_{\max} (Z) [\alpha_1^2 (Z) + \alpha_2^2 (Z)]}{D \alpha_2 (Z) \alpha_1^2 (Z)} \sin \frac{L G_1 (Z) \alpha_2 (Z)}{G_1 (Z) + G_2 (Z)} \quad (5)$$

where Z is a series of factors including CP, moisture content, dry density of soil, and so forth. Apparently, if σ_{\max} is larger than σ_y under a specific condition, the strain sensing fiber may undergo plastic deformation when measuring soil deformation. Given that the relationship between model parameters (τ_{\max} , G_1 , and G_2) and various environmental factors Z have been obtained using sufficient experimental data, one may estimate the maximum tensile stress that may exist within a fiber for a given environmental condition. It is noteworthy that Eq. (5) is only a criterion for determining whether or not a POF may undergo plastic deformation, and the maximum tensile stress will not exceed the tensile strength under real conditions.

4.2 Plasticity effect on soil deformation monitoring

According to the stress–strain curve for the PMMA POF shown in Fig. 2, the stress increased approximately linearly with the strain up to the yield point, afterwards the strain increased continuously without significant increase in the stress. For a preliminary analysis, the stress–strain relationship of the PMMA POF may be assumed to be ideal elastoplastic, as shown in Fig. 10. Briefly, prior to the yield point the fiber will deform elastically and will recover all its strain upon unloading; however, if the fiber is unloaded after reaching the yield point, it will recover its elastic strain component but a permanent set will remain. As a result, this property may bring uncertainties to the measurements.

As described previously, if $\sigma_{\max} < \sigma_y$ the POF is able to properly function until the fiber–soil interface is debonded due to increased deformation of the surrounding soil. Under the circumstance of $\sigma_{\max} \geq \sigma_y$, however, the fiber yields prior to the debonding of the interface. In this case, once σ_y is reached the tensile stress will redistribute within the fiber, and, of course, the strain will redistribute as well. Moreover, if the soil deformation decreases, the variation may

not be captured by the fiber because only part of its deformation can be recovered. In this case, the measured strain due to soil deformation is distorted or overestimated. Geotechnical engineers should pay special attention to this issue because the deformation pattern of geo-structures can be very complex due to complicated construction conditions and geologic environment.

Fig. 11 schematically shows the deformation–time curves of two model soil slopes under different environmental conditions. In Case 1, a slope was excavated in stages. Notably, no decrease of deformation was observed during the entire process of excavation. In contrast, the deformation of the slope in Case 2 increased and decreased due to the fluctuation of water level. Importantly, for situations where the deformation increases continuously and induces plastic deformation of a POF, the deformation can be captured as long as the light guiding properties are maintained. However, if the deformation suddenly decreases, the decrease may not be recorded by the POF provided that the variation is larger than the elastic deformation of the POF.

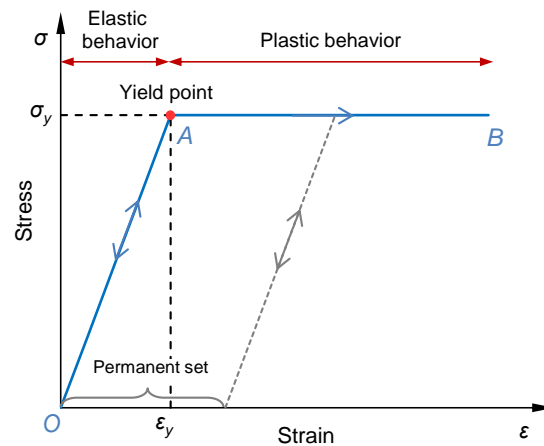


Fig. 10 Ideal elastoplastic shear stress–strain relationship for a PMMA POF simplified from the measured stress–strain curve shown in Fig. 1

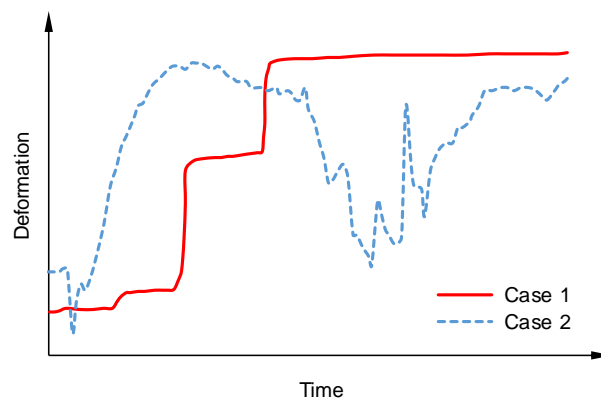


Fig. 11 Schematic deformation–time curves of two model soil slopes under different environmental conditions. Case 1: three-stage excavation at slope toe, and Case 2: complex water level fluctuation

5. Conclusions

This paper describes a first attempt to understand the mechanical interaction between POF and soil. Pullout tests were performed to study the load–deformation properties of a 2.2 mm jacketed PMMA POF embedded in soil. CPs ranging from 7.5 kPa to 90 kPa were investigated. The data were interpreted using a simplified fiber–soil interaction model, and were compared with previously reported SOFs data. The results showed that the CP range used in this study did not induce plastic deformation of the POF. Moreover, the POF–soil interface and the SOF–soil interface shared more similarities than differences under the current experimental conditions. Additionally, these results revealed an important role for CP in control of the fiber–soil interfacial bond and the fiber measurement range. Similar to the SOF, high CPs enhanced the interfacial bond between the POF and the surrounding soil, and widened the measurement range of the POF.

An expression for the maximum tensile stress that may exist in a fiber was formulated. Given a specific environmental condition, one may use this expression to estimate whether a POF will undergo plastic deformation when measuring soil deformation. The plastic deformation of POF may influence the reliability of measured fiber optic data, especially for monitored geo-structures whose deformation alternately increases and decreases.

Taking all these data and discussions together, we conclude that the mechanical behavior of a PMMA POF–soil interface is similar to a SOF–soil interface, although it cannot be excluded at this stage that plastic deformation of the fiber may contribute to complex fiber–soil interactions under certain circumstances. Furthermore, in terms of the interfacial parameters studied here, the PMMA POF is suitable for monitoring of soils and geotechnical-related structures, as long as the plastic deformation issue is carefully addressed.

Acknowledgments

This work was supported by the National Natural Science Foundation of China (Grant No. 41302217), the National Key Technology R&D Program of China (Grant No. 2012BAK10B05), and the Suzhou Science and Technology Development Program (Grant No. SYG201213). The corresponding author would like to acknowledge the financial support from the China Scholarship Council for his one-year academic visit to the University of Cambridge. Thanks are also given to Jin-Wen Huo and Tian-Ding Wang for their help in the laboratory experiments.

References

- Abdi, O., Kowalsky, M., Hassan, T., Kiesel, S. and Peters, K. (2008), “Large deformation polymer optical fiber sensors for civil infrastructure systems”, *Proc. SPIE*, **6932**, 693242.
- Arifin, A., Hatta, A.M., Muntini, M.S. and Rubiyanto, A. (2015), “Long-range displacement sensor based on SMS fiber structure and OTDR”, *Photonic Sens.*, **5**(2), 166-171.
- ASTM. (1992), “Standard test method for classification of soils for engineering purposes (unified soil classification system)”, D2487-90, West Conshohocken, PA.
- Bilro, L., Alberto, N., Pinto, J.L. and Nogueira, R. (2012), “Optical sensors based on plastic fibers”, *Sensors*, **12**(9), 12184-12207.
- Feng, X., Wu, W.J., Li, X.Y., Zhang, X.W. and Zhou, J. (2015), “Experimental investigations on detecting lateral buckling for subsea pipelines with distributed fiber optic sensors”, *Smart Struct. Syst.*, **15**(2),

- 245-258.
- Glisic, B. and Yao, Y. (2012), "Fiber optic method for health assessment of pipelines subjected to earthquake-induced ground movement", *Struct. Health Monit.*, **11**(6), 696-711.
- Grassini, S., Ishtaiwi, M., Parvis, M. and Vallan, A. (2014), "Design and Deployment of low-cost plastic optical fiber sensors for gas monitoring", *Sensors*, **15**(1), 485-498.
- Habel, W.R. and Krebber, K. (2011), "Fiber-optic sensor applications in civil and geotechnical engineering", *Photonic Sens.*, **1**(3), 268-280.
- Iten, M., Puzrin, A.M. and Schmid, A. (2008), "Landslide monitoring using a road-embedded optical fiber sensor", *Proc. SPIE*, **6933**, 693315.
- Klar, A., Dromy, I. and Linker, R. (2014), "Monitoring tunneling induced ground displacements using distributed fiber-optic sensing", *Tunn. Undergr. Sp. Tech.*, **40**, 141-150.
- Krebber, K., Lenke, P., Liehr, S., Witt, J. and Schukar, M. (2008), "Smart technical textiles with integrated POF sensors", *Proc. SPIE*, **6933**, 69330V.
- Kuang, K.S.C. (2015), "Distributed damage detection of offshore steel structures using plastic optical fiber sensors", *Sens. Actuat. A - Phys.*, **229**, 59-67.
- Kuang, K.S.C., Quek, S.T., Koh, C.G., Cantwell, W.J. and Scully, P.J. (2009), "Plastic optical fibre sensors for structural health monitoring: a review of recent progress", *J. Sensors*, **2009**, 312053.
- Large, M.C., Moran, J. and Ye, L. (2009), "The role of viscoelastic properties in strain testing using microstructured polymer optical fibres (mPOF)", *Meas. Sci. Technol.*, **20**(3), 034014.
- Lenke, P., Liehr, S., Krebber, K., Weigand, F. and Thiele, E. (2007), "Distributed strain measurement with polymer optical fiber integrated in technical textiles using the optical time domain reflectometry technique", *Proceedings of the 16th Int. Conf. on Plastic Optical Fibre*, 21-24.
- Leung, C.K., Wan, K.T., Inaudi, D., Bao, X., Habel, W., Zhou, Z., Ou, J., Ghandehari, M., Wu, H.C. and Imai, M. (2013), "Review: Optical fiber sensors for civil engineering applications", *Mater. Struct.*, **48**(4), 871-906.
- Li, M., Zhang, G., Zhang, J.M., and Lee, C.F. (2011), "Centrifuge model tests on a cohesive soil slope under excavation conditions", *Soils Found.*, **51**(5), 801-812.
- Liehr, S., Lenke, P., Krebber, K., Seeger, M., Thiele, E., Metschies, H., Gebreselassie, B., Münich, J.C. and Stempniewski, L. (2008), "Distributed strain measurement with polymer optical fibers integrated into multifunctional geotextiles", *Proc. SPIE*, **7003**, 700302.
- Liehr, S., Lenke, P., Wendt, M., Krebber, K., Seeger, M., Thiele, E., Metschies, H., Gebreselassie, B. and Münich, J.C. (2009), "Polymer optical fiber sensors for distributed strain measurement and application in structural health monitoring", *IEEE Sens. J.*, **9**(11), 1330-1338.
- Ling, H.I., Wu, M.H., Leshchinsky, D., and Leshchinsky, B. (2009), "Centrifuge modeling of slope instability", *J. Geotech. Geoenviron. Eng.*, **135**(6), 758-767.
- Mohamad, H., Soga, K., Bennett, P.J., Mair, R.J. and Lim, C.S. (2012), "Monitoring twin tunnel interaction using distributed optical fiber strain measurements", *J. Geotech. Geoenviron. Eng.*, **138**(8), 957-967.
- Morisawa, M. and Muto, S. (2012), "Plastic optical fibre sensing of fuel leakage in soil", *J. Sensors*, **2012**, 247851.
- Naruse, H., Uchiyama, H., Kurashima, T. and Unno, S. (2000), "River levee change detection using distributed fiber optic strain sensor", *IEICE Trans. Electron.*, **E83-C**(3), 462-467.
- Olivares, L., Damiano, E., Greco, R., Zeni, L., Picarelli, L., Minardo, A., Guida, A. and Bernini, R. (2009), "An instrumented flume for investigation of the mechanics of rainfall-induced landslides in unsaturated granular soils", *Geotech. Test. J.*, **32**(2), 108-118.
- Peters, K. (2011), "Polymer optical fiber sensors—a review", *Smart Mater. Struct.*, **20**(1), 013002.
- Sharma, J.S. and Bolton, M.D. (2001), "Centrifugal and numerical modelling of reinforced embankments on soft clay installed with wick drains", *Geotext. Geomembr.*, **19**(1), 23-44.
- Sun, Y.J., Zhang, D., Shi, B., Tong, H.J., Wei, G.Q. and Wang, X. (2014), "Distributed acquisition, characterization and process analysis of multi-field information in slopes", *Eng. Geol.*, **182A**, 49-62.
- Tang, C.S., Shi, B. and Zhao, L.Z. (2010), "Interfacial shear strength of fiber reinforced soil", *Geotext. Geomembr.*, **28**(1), 54-62.

- Wang, B.J., Li, K., Shi, B. and Wei, G.Q. (2009), "Test on application of distributed fiber optic sensing technique into soil slope monitoring", *Landslides*, **6**(1), 61-68.
- Zeni, L., Picarelli, L., Avolio, B., Coscetta, A., Papa, R., Zeni, G., Di Maio, C., Vassallo, R. and Minardo, A. (2015), "Brillouin optical time-domain analysis for geotechnical monitoring", *J. Rock Mech. Geotech. Eng.*, **7**(4), 458-462.
- Zhang, C.C., Zhu, H.H., She, J.K., Zhang, D. and Shi, B. (2015), "Quantitative evaluation of optical fiber/soil interfacial behavior and its implications for sensing fiber selection", *IEEE Sens. J.*, **15**(5), 3059-3067.
- Zhang, C.C., Zhu, H.H., Shi, B. and She, J.K. (2014), "Interfacial characterization of soil-embedded optical fiber for ground deformation measurement", *Smart Mater. Struct.*, **23**(9), 095022.
- Zhu, H.H., Ho, A.N.L., Yin, J.H., Sun, H.W., Pei, H.F. and Hong, C.Y. (2012), "An optical fibre monitoring system for evaluating the performance of a soil nailed slope", *Smart Struct. Syst.*, **9**(5), 393-410.
- Zhu, H.H., Shi, B., Yan, J.F., Zhang, J. and Wang, J. (2015), "Investigation of the evolutionary process of a reinforced model slope using a fiber-optic monitoring network", *Eng. Geol.* **186**, 34-43.
- Zhu, H.H., Shi, B., Zhang, J., Yan, J.F. and Zhang, C.C. (2014), "Distributed fiber optic monitoring and stability analysis of a model slope under surcharge loading", *J. Mt. Sci.*, **11**(4), 979-989.